ENHANCED KNOWLEDGE IN SCIENCES AND TECHNOLOGY
e-ISSN: 2773-6385

EKST

Vol. 4 No. 2 (2024) 482-487
https://publisher.uthm.edu.my/periodicals/index.php/ekst

Stainless Steel Metal Corrosion Induction by Water Contained Sulphur in Geothermal Well

Nurul Nabila Ermyra Ellysha[1], Zaidi Embong[1]*, Khawarizmi Jafery[1]

[1] *Department of Physics and Chemistry, Faculty of Applied Science and Technology, Universiti Tun Hussein Onn Malaysia, 84600 Pagoh, Johor, Malaysia*

*Corresponding Author: zaidi@uthm.edu.my
DOI: https://doi.org/10.30880/ekst.2024.04.02.053

Article Info

Received: 27 December 2023
Accepted: 12 January 2024
Available online: 12 December 2024

Keywords

Corrosion

Abstract

The study investigates the impact of sulfur on the corrosion of stainless-steel samples immersed in geothermal hot spring water. Stainless steel, known for its corrosion resistance due to forming a protective oxide layer, faces challenges in geothermal environments, exacerbated by sulfur compounds. Several analysis methods such as SEM-EDX, FTIR, and Raman Spectroscopy were employed for chemical property analysis. After 7 days of immersion, SEM-EDX revealed initial corrosion with cracks and grains, progressing to severe damage after 14 days. FTIR analysis detected some functional groups in the geothermal water sample, including amine group (N-H), thiocyanate (S-C=N), sulfoxide (S=O), phenol group (O-H) while Raman Spectroscopy identified molecular structure of corrosion products on the steel surface and revealed that several oxides were found in the analysis such as α-FeOOH(goethite), γ-FeOOH (lepidocrocite) and Fe_3O_4 (magnetite). The study provides crucial insights into the corrosion processes at both microand molecular levels,addressing the durability issues of stainless steel ingeothermal power generation.

1. Introduction

Geothermal energy harnesses heat from the Earth's interior for various applications, including cooking, bathing, heating, and electricity production. Surface features like geysers and hot springs are manifestations of the Earth's core heat, generated by radioactive decay and friction along plate borders. Geothermal energy is also employed for cooking, industrial processes, milk pasteurization, and snow melting, primarily utilizing hot water either alone or with heat exchange when dealing with unfavorable minerals and gases [3]. Geothermal fluids from the Earth's upper crust, associated with active volcanism, yield 3-5 MW of electric power per well. Reservoir fluid temperatures range from 230 to 350 °C, and some aquifers are highly pressured. Enthalpy, representing the fluid's overall energy, is a key consideration. Well-testing provides crucial information about reservoir conditions. Geothermal wells differ significantly from oil and gas wells, exposing formations along the entire open-hole section, with potential depths as large as 2000 m [4].

Through well testing, which offers information about the conditions of the reservoir and makes it possible to gauge manufacture well production or re-injection well capacity, wells are the main path into the underground reservoir. There are numerous significant ways that geothermalwells different from those dug in oil and gasexploration. In geothermal wells, the potentially effective formations get exposed to thewellbore throughout the entire open-hole section, whereas in oil and gas wells, the producing zone is typically limited to a small, well-defined vertical interval. This is oneof the most important distinctions between geothermal wells and gas and oil wells. Geothermal wells may have an open-hole section as large as 2000 m [5].

Corrosive acids in geothermal fluids, such as sulfuric, hydrochloric, or hydrofluoric acid, cause severe surface corrosion [6]. Epoxy-coating steel surfaces can provide a defense. Material choice is crucial for the long service life of geothermal systems, with mild steel known for non-corrosive fluids. Examining corrosion includesthe study of surface texture, and impacting material characteristics like resistance to friction and wear. While most geothermal liquids are not corrosive, surface texture plays a crucial role in the choice of materials for casing and pipe construction [7].

On the other hand, some issues are involved in geothermal water which is the main source of geothermal energy as most geothermal operations experience corrosion attacks, which severely damage the equipment. Extreme geothermal vapor and brine corrosion tendencies affect production wells, steam and brine collection systems, injection lines, and wells. Due to geothermal steam's chemical composition, steam turbines frequently experience stress corrosion cracking as well. These equipment and pipe failure in the systems is a result of several modes of corrosion attack [8].

Therefore, this research has focused on the results of corrosion research for metal that was conducted ina geothermal well simulation of a superheated geothermal environment to investigate the corrosion attack by sulfur compounds on the metal surface in the geothermal well.

2. Materials and Methods

In this corrosion study, geothermal water from Jasin, Melaka, was utilized to assess the impact on stainless steel samples. The experiment employed two exposure configurations: one submerged for 7 days and another for 14 days, maintaining a constant water temperature. The stainless-steel samples, measuring 10mm x 10mm x 3mm, underwent surface preparation through polishing and were characterized for pre-corrosion composition using Scanning Electron Microscopy and energy-dispersive X-ray analysis. Immersion tests were conducted in a shaking incubator set at 43°C for 7 and 14 days as shown in Fig. 2.1 below. Post-immersion analysis includedRaman spectroscopy, SEM-EDX, and FTIR to evaluate changes in both physical and chemical properties. The study aimed to identify corrosion products and their crystal structure, employing advanced imaging and analytical techniques to compare pre and post-corrosion characteristics.

Fig. 2.1 *Immersion test set up inside the shaker incubator at a constant temperature.*

To initiate the immersion tests, stainless steel coupons with dimensions of 10mm x 10mm x 3mm were prepared. After washing with distilled water, cleaning with ethyl alcohol, and air drying at room temperature, the coupons were immersed in geothermal water within a conical flask. The temperature was maintained at the geothermal well's level, and the samples were shaken inside an incubator at 60 revolutions per minute and 43°C for 7 and 14 days. The samples underwent analysis before and after the immersion test, utilizing Raman Spectroscopy, Scanning Electron Microscopy with Energy Dispersive X-ray Spectroscopy (SEM-EDX), and Fourier-transform Infrared Spectroscopy (FTIR). Advanced imaging and analysis techniques were applied to assess surface and cross-sectional morphology, elemental mapping, and crystal structures of the corroded metal samples [9]. This comprehensive approach allowed for a thorough examination of the corrosion behavior and characteristics of the stainless-steel samples in water.

Enhanced Knowledge in Sciences and Technology Vol. 4 No. 2 (2024) p. 482-487

3. Result and Discussions

3.1 Scanning Electron Microscopy and Energy Dispersive X-ray Analysis of Stainless-steel Sample.

The immersion experiments extended from 7 to 14 days, and the corrosion product's morphology on the surface was examined using an optical microscope. Surface texture, identified as the preferred orientation, was a crucial factor in the corrosion research. Scanning electron microscopy in Fig. 3.1 depicted the evolution of the surface after the immersion test. The raw stainless-steel sample exhibited a heterogeneous surface due to abrasive paper polishing, showing lamina line formation and a smooth, uniform surface withoutmacroscopic defects. Elemental analysis identified elements like Iron (Fe), Chromium (Cr), Nickel (Ni), and Oxygen (O) on the surface.

After 7 days of immersion (Fig. 3.1(b)), cracks and pores developed, indicating severe corrosion. The elemental composition showed a decrease in Cr and Ni, suggesting corrosion, while the atomic percentage of Oxygen increased, indicating oxidation. After 14 days (Fig. 3.1(c)), severe damage was observed, with brittles and cracks reduced but some porosity remaining. Elemental analysis revealed an increase in Iron (Fe) and Chromium (Cr) and a decrease in Oxygen (O), supporting the idea that the metal surface slowly returned to its raw morphology as corroded layers were removed. The data emphasized that when metal corrodes, it reacts with oxygen, reducing the atomic percentage of oxygen and leading to the deterioration of the metal surface [10].

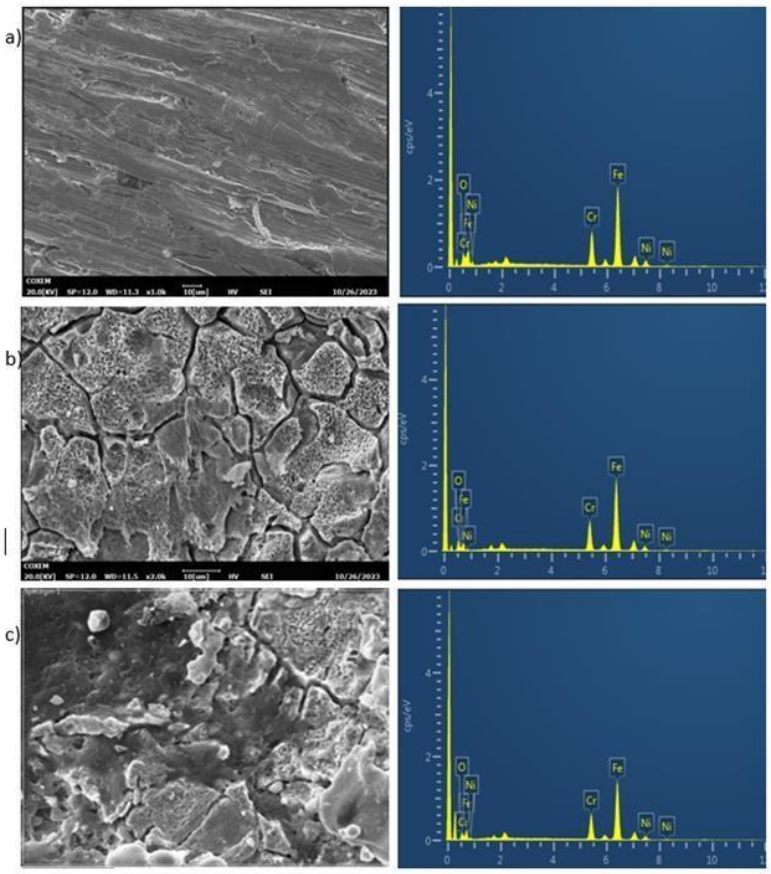

Fig. 3.1 *Morphology and Elemental analysis of the raw sample(a), 7 days sample(b), and 14 days sample(c).*

3.2 Fourier Transform Infrared Analysis of Water Sample.

Fourier transform infrared (FTIR) analysis was employed to characterize the surface of atmospherically exposed metal plates, focusing on corrosion films formed during the early stages of air corrosion. Chemical reactions between the metal substrate and adsorbed gases, as well as reactions between corrosion products and adsorbed gases, lead to the formation of layers of corrosion products [11]. The FTIR analysis evaluated the functional groups present in the sample within the wavelength range of 1100-3900 cm^{-1}.

Fig. 3.2 displays spectra obtained from the analysis of the geothermal water sample. The various spectra highlight unique spectral features corresponding to abundant functional groups in the FTIR spectrum of the steel sample, including amine group (N-H), thiocyanate(S-C=N), sulfoxide (S=O), and phenol group (O-H). The intensive IR absorption bands of the hydrogen group are notable. Key FTIR peaks were observed at 3381 cm^{-1}. (N-H stretching of aliphatic primary amine), 2146 cm^{-1} (thiocyanate with S-C≡N group), and 1319 cm^{-1}. (sulfoxide, S=O, and phenol, O-H, vibration at medium range). The FTIR analysis provided valuable insights into the functional groups present on the metal surface exposed to geothermal water.

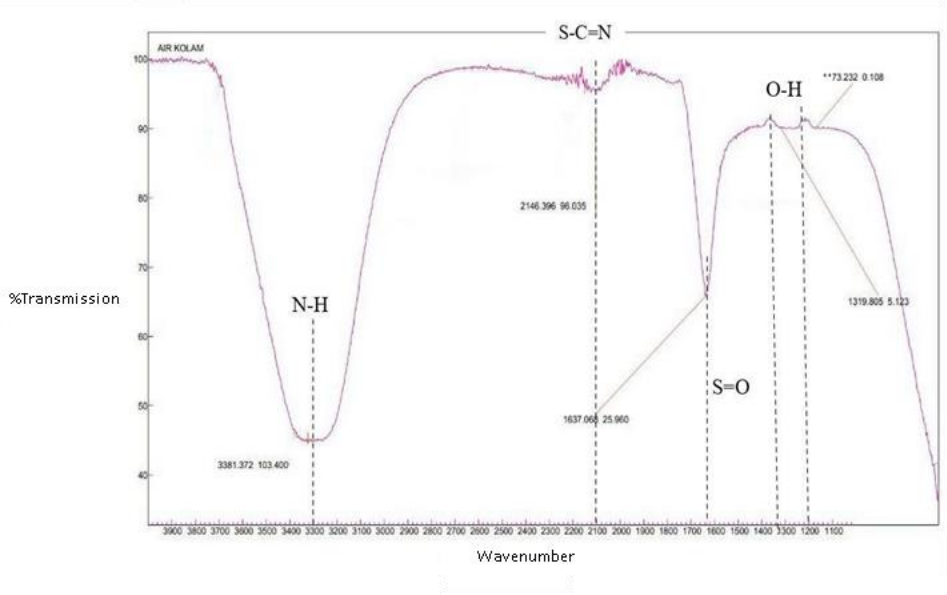

Fig. 3.2 *FTIR spectrum for a geothermal water sample.*

3.3 Raman Spectroscopy Analysis of Sample Surface Compound.

The resulting Raman spectrum was plotted as intensity versus Raman shift. The shift in frequency between the incident light and the scattered light is represented by the x-axis, which is also referred to as the Raman shift. It expresses the energy differential between the incident and scattered photons. It is measured in wavenumbers (cm to the, minus 1 end superscript.) while the intensity of the Raman scattered light is shown on the y-axis. It provides information about the Raman scattering signal's strength or magnitude at a specific Raman shift [12]. There are several oxides were found in this analysis such as FeOOH(goethite), γ-FeOOH(lepidocrocite), and F Fe_3O_4 (magnetite). Goethite, or α-, FeOOH produces comparatively prominent peaks in the spectra at wavenumber 200 cm-1 as seen in Figure 3.3. These results are generally in good agreement with the values reported in Table 3.1. Lepidocrocite, or γ-FeOOH, has a peak at 900 cm^{-1} . Fe_3O_4 or magnetite, exhibits a prominent spectrum that indicates the presence of a chemical reaction during the corrosion process that converts Iron (Fe) into magnetite.

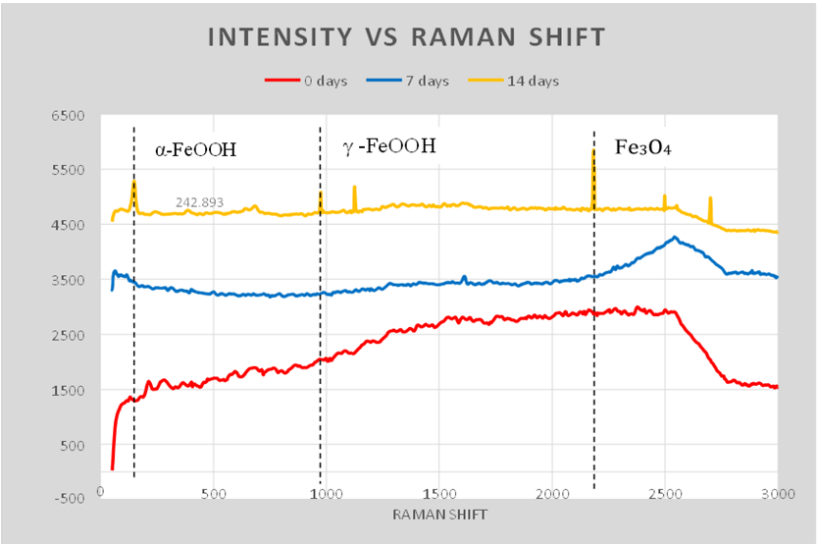

Fig. 3.3 *Intensity vs Raman Shift graph of Raman analysis for stainless-steel sample.*

Table 3.1 *Raman wavenumbers for iron oxide phases used in this study [10].*

Oxides	Wavenumbers (cm^{-1})
$Fe(OH)_2$	460,550
$Fe(OH)_3$	395,696,1335,692
α-FeOOH	245,300,390,420,480,550,685,248,303,397,485,554,680,1002,1120,245,300,390,485,550,675,900
β-FeOOH	310,386,497,538,723,310,385,415,480,535,615,675,725
γ-FeOOH	255,380,528,654,1054,1307,252,380,660
δ-FeOOH	400,655,220,295,385
α-Fe_2O_3	227,245,293,298,414,501,612,225,245,295,415,500,615,1320
γ-Fe_2O_3	265,300,345,515,645,670,715,1440,350,505,660,710,1425
Fe_3O_4	616,663,298,319,418,550,676,1322,2500,2650

4. Conclusion

In the study of stainless-steel corrosion in geothermal water with a pH of 6 and a temperature of 43°C, various analytical techniques were employed. Raman analysis identified corrosion molecular structures, including α-FeOOH (goethite), γ-FeOOH (lepidocrocite), and Fe3O4 (magnetite). Fourier-transform infrared (FTIR) analysis revealed distinctive spectral features corresponding to functional groups such as N-H, S-C=N, S=O, and O-H. Scanning electron microscopy (SEM) results illustrated the progression of corrosion, indicating the formation of a thicker oxide layer, sandy and circular grains, cracks, bird's nests, and brittles, representing lepidocrocite, goethite, and magnetite. Pre- corrosion stainless steel exhibited a non-homogeneous surface. Energy-dispersive X-ray spectroscopy (EDX) analysis confirmed the main element composition of the corrosion product as Fe and Cr. Overall, the combined effect of slightly acidic conditions, elevated temperature, and specific corrosion products contributed to the severe corrosion observed on the stainless-steel surface immersed in geothermal water.

Acknowledgement

The authors would like to thank the Faculty of Applied Sciences and Technology, Universiti Tun Hussein Onn Malaysia, for its support in completing this project.

Conflict of interest

Authors declare there is no conflict of interests regarding the paper's publication.

Author Contribution

The authors confirm contribution to the paper as follows: ***study conception and design, data collection, methodology, analysis and interpretation of results:*** *Nurul Nabila Ermyra Ellysha, Zaidi Embong and Khawarizmi Jafery. All authors reviewed the results and approved the final version of the manuscript.*

References

[1] A. Nganga, S. Thórhallsson, I. Örn Thorbjörnsson, and G. Skúlason Kaldal, "Geothermal Well Design Using the New 2015 New Zealand Standard and 1991 Standard A Case of MW-20A in Menengai, Nakuru County, Kenya," 2017. [Online]. Available: https://www.researchgate.net/publication/355856222
[2] C. I. Igwe, "Geothermal Energy: A Review Development and Evaluation of an Electrolyzer for Production of Hydrogen and Electrical Energy in a Fuel Cell View project," 2021. [Online]. Available: https://www.researchgate.net/publication/350823763
[3] M. A. Grant and P. F. Bixley, Geothermal reservoir engineering. AcademicPress, 2011.
[4] G. Smoot, "What is the carbon footprint of geothermal energy? A life-cycle assessment," 2023.
[5] G. Up, "The Effects and Economic Impact of Corrosion," Corros. Underst. Basics, pp. 1–20, 2019.
[6] M. A. Azam, S. Sukarti, and M. Zaimi, "Corrosion behavior of API-5L-X42 petroleum/natural gas pipeline steel in South China Sea and Strait of Melaka seawaters," Eng. Fail. Anal., vol. 115, no. June, pp. 1–8, 2020,
[7] S. Nitonye, U. O. Emmanuel, and A. O. Ezenwa, "Combating Corrosion in Transmission Pipelines in Marine Environment Using Vernomia Amydalina as Inhibitor," Open J. Mar. Sci., vol. 08, no. 04, pp. 450–472, 2018,

[8] S. Prifiharni, L. Nuraini, G. Priyotomo, Sundjono, H. Gunawan, and I. Purawiardi, "Corrosion performance of steel and galvanized steel in geothermal water environment," AIP Conf. Proc., vol. 1964, no. May, 2018,
[9] R. A. S. A. Mardhiah I, Norharzilan Y, Abdulhah A, Rasol, R, "Effect of pH corrosion sulfate reducing Mardhiah 2014.pdf," Journal of environmental science and technology. pp. 209–217, 2019
[10] Eli Mendy 'Raman Database open source for material analysis'," 2020.
[11] E. Matsubara, S. Suzuki, and Y. Waseda, "6 Corrosion Mechanism of Iron from an X-ray Structural Viewpoint."
[12] A. Toloei, V. Stoilov, and D. Northwood, "The relationship between surface roughness and corrosion," in ASME International Mechanical Engineering Congress and Exposition, Proceedings (IMECE), American Society of Mechanical Engineers (ASME), 2013.